Materials Chemistry and Physics 119 (2010) 40–47

Contents lists available at ScienceDirect

Materials Chemistry and Physics

journal homepage: www.elsevier.com/locate/matchemphys

Various curing conditions for controlling PTFE micro/nano-fiber texture of a bionic superhydrophobic coating surface

Zhuangzhu Luo[a,b], Zhaozhu Zhang[a,*], Wenjing Wang[a], Weimin Liu[a,*], Qunji Xue[a]

[a] State Key Laboratory of Solid Lubrication, Lanzhou Institute of Chemical Physics, Chinese Academy of Sciences, Lanzhou 730000, PR China
[b] Graduate School, Chinese Academy of Sciences, Beijing 100039, PR China

ARTICLE INFO

Article history:
Received 4 February 2009
Received in revised form 26 May 2009
Accepted 19 July 2009

Keywords:
Polytetrafluoroethylene (PTFE)
Polymer micro/nano-fiber
Curing condition
Superhydrophobicity
Controllable

ABSTRACT

A simple and conventional coating-curing process to fabricate superhydrophobic coating surface with both the micro-nano-scale binary structure (MNBS) roughness, and the lowest surface energy hydrophobic groups ($-CF_3$) on engineering materials of stainless steel or other metals was developed by control of curing conditions. Results show that higher temperature and longer cooling time resulted in longer crystallizing process, and the forming PTFE aggregates could slowly produce the crystallization and create the willow-leaf-like or wheat-haulm-leaf-like polymer micro/nano-fiber on the atop surface. The curing temperature dramatically influences the micro/nano-fiber texture of the PTFE/PPS superhydrophobic coating surface, leading to the excellent superhydrophobicity at higher temperature. An increase of the curing temperature is beneficial to fluorine gradient-distribution, PPS thermal-oxidative cross-linking and oxidative reaction, resulting in the enhancement of adhesive strength and mechanical properties of the PTFE/PPS superhydrophobic coatings. A bionic superhydrophobic surface with porous gel-like network and PTFE micro/nano-fiber textures could be created by natural cooling in air, whereas PTFE nano-sphere/-papillates textures could be fabricated by hardening in H_2O.

1. Introduction

Superhydrophobicity is a wetting phenomenon, capable of exhibiting high water contact angles (WCAs) up to $162 \pm 5^\circ$ and very low water sliding angles (WSAs) [1–5]. Such interface behavior allows rain droplets to simply roll off from the surfaces, thus rinsing the dirt and debris from the surfaces, i.e., "*self-cleaning*" or "*lotus effect*." It is attributed to the existence of the micro-nano-scale binary structure (MNBS) roughness and/or the low surface energy hydrophobic groups [6–10].

Because of the potential practical applications, superhydrophobic surfaces with WCAs larger than 150° and low WSAs have aroused the fantasy of many researchers [11–16]. Synthetic superhydrophobic surfaces have been fabricated by various approaches through controlling the surface topography of expensive hydrophobic materials, including creating a rough surface covered with low surface energy molecules, etching the surface of hydrophobic materials, and generating well-ordered microstructured surfaces [17–28]. However, these methods for creating superhydrophobic surfaces usually use expensive materials or be prepared at severe conditions, limiting the practical applications of superhydrophobic surfaces. Bionic polymer surfaces with superhydrophobicity by one-step casting process under an ambient atmosphere have been prepared on glass substrate [29–33]. However, it is well-known that the various superhydrophobic surfaces were only fabricated on the glass substrates under room (or low) temperature, and their adhesive strength between polymer coatings and glass substrates was weak, easily scraped off, and with shorter stability over low or high temperature in comparison with that of prepared at high temperature [29–33].

In our previous work, we demonstrated that the bionic PTFE/PEEK superhydrophobic coating [34] and PTFE/PPS superhydrophobic/hydrophobic coating surfaces [35,36] with long-term stability, strong cohesive strength and anti-temperature change were prepared by a simple, inexpensive and conventional coating-curing process. However, the effects of the curing conditions on the MNBS roughness and the distribution of low surface energy hydrophobic groups of the superhydrophobic/hydrophobic coating surface were not systematically investigated. In the present work, the PTFE/PPS superhydrophobic coating was prepared under various curing temperatures and cooling conditions, the changes of the MNBS roughness and the gradient-distribution of the hydrophobic groups in the superhydrophobic coating were investigated in further detail. The mechanism of the controllable fabrication of PTFE nano-fiber/-sphere and MNBS texture was discussed and demonstrated.

* Corresponding authors. Tel.: +86 931 4968098; fax: +86 931 4968098.
E-mail addresses: zzzhang@lzb.ac.cn (Z. Zhang), wmliu@lzb.ac.cn (W. Liu).

0254-0584/$ – see front matter.
doi:10.1016/j.matchemphys.2009.07.039

2. Experimental details

2.1. Materials

Superhydrophobic surfaces were fabricated through engineering materials, such as stainless steel or other metal substrates, by using PTFE, PPS in mixed solvent (distilled water/ethanol/isobutyl alcohol in a volume fraction of 2:5:1), non-ionic surfactant (octyphenol polyoxyethylene ether: C_8H_{17}-Ph-O$(C_2H_4O)_nH$, $n \sim 10$) and ammonium carbonate ($(NH_4)_2CO_3$).

2.2. Fabrication of PTFE/PPS superhydrophobic coating

The chemical composition of stainless steel (1Cr18Ni9Ti) includes ≤0.12 wt.% carbon, 17–19 wt.% chromium, 8–11 wt.% nickel, 0.5–0.8 wt.% titanium, balance iron. The stainless steel block was polished with 500# and 900# sand papers in turn, and then cleaned with acetone in an ultrasonic bath for 5 min. The commercially available PTFE powder with low surface energy was dispersed in the mixed solvent, 10 wt.% non-ionic surfactant and 0.5 M $(NH_4)_2CO_3$ solution with ultrasonic stirring for 30 min, and then the PTFE emulsion (O/W) were obtained. PPS resin was selected as the binding agent. And then, the binder were mixed into the PTFE emulsion and dispersed for 10 min, and allowed the formation of coating precursors. The wet coatings on stainless steel or various metal substrate blocks were prepared by spraying the coating precursors with 0.2 MPa nitrogen gas and curing at temperature 150 °C for 1 h and 340–400 °C for 1.5 h. The thickness of the wet coatings was controlled by regulating the spraying speed and the composition of non-volatile constituents in the coating precursors.

2.3. Curing conditions

The wet coatings on stainless steel or other metals substrate blocks were cured at temperature of 150 °C for 1 h, and of 340 °C, 360 °C, 370 °C, 380 °C, 390 °C and 400 °C for 1.5 h, after that naturally cooled in air to room temperature, respectively. Moreover, the wet coatings were cured at temperature of 380 °C for 1.5 h and then cooled in water (that is, hardening in H_2O). The thickness of the cured PTFE/PPS composite coatings was measured with a MINITEST 1100 Microprocessor Coating Thickness Gauge (Elektro-Physik, Koln). Tests show that thickness of the cured coating could range from 5 μm to 100 μm.

2.4. Characterization

The microstructures of the coating surface obtained at various curing temperatures and cooling process were observed by scanning electron microscopy (SEM, JSM-5600LV). X-ray photoelectron spectroscopy (XPS) analysis of the sample was performed on a VG ESCALAB 210 (VG Scientific) spectrometer with an Mg Kα X-ray source (1253.6 eV). Contact angles and sliding angles of 5–15 μl water droplets on the coating surface were measured with a CA-A contact angle meter at ambient temperature (CA-A, Kyowa Scientific Co. LTD, Japan). The average WCA and WSA values were determined by measuring at five different positions of the same sample and their images were captured with a traditional digital camera (Canon).

3. Results and discussion

3.1. The control of the MNBS by curing temperature

Fig. 1 shows the effect of the curing temperature on the WCA and WSA of the PTFE/PPS superhydrophobic surfaces upon stainless steel substrate, respectively. It can be clearly seen that the WCA increases slightly with increasing curing temperature up to approximately at 370 °C and then increases sharply. The WCA changed from about 155° to 159° and the WSA from 13° to 10°, respectively, when the curing temperature increased from 340 °C to 370 °C. At the highest curing temperature up to about 400 °C, the PTFE/PPS superhydrophobic coating surface has the largest WCA with about 169° and the smallest WSA of about 3° (similar to the WSA of the lotus leaf), and water droplets could be moved upward easily even if the surface is only slightly tilted or shaken. Accordingly, the PTFE/PPS superhydrophobic coatings cured at higher temperature possess better superhydrophobicity.

The PTFE/PPS superhydrophobic coatings cured at various temperatures have different WCAs and WSAs, which correspond with the MNBS structure of the surfaces, as shown in Fig. 2. It can be clearly seen that the porous networks, micro-papillaes or -islands, and micro-structure (Fig. 2a, c, e and g) of the surfaces cured at various temperatures are very similar. The micro-papillaes or -islands with diameters of 5–30 μm are distributed uniformly across the porous network surfaces, as shown in Fig. 2(a, c, e and g). However, the micro/nano-fluorocarbon fiber textures of the surfaces cured at various temperatures are very different in sizes and shapes. When the curing temperature was at 340 °C, the density of the nano-fiber textures was sparse (Fig. 2b), and the size of nano-fiber was thin and short, which resulted in the low WCA of about 155° (Fig. 3a) and high WSA of about 13° on the coating surfaces. As the curing temperature increased up to 380 °C, the density of the nano-fiber textures was thick (Fig. 2d), and the size of nano-fiber was wide and long. These obtained micro/nano-fibers initiated cross-linking each other and formed networks with micro/nano-pores and -apertures on the coating atop, resulting in higher WCA with about 162° (Fig. 3b) and smaller WSA of about 6° on the atop surfaces. The shape of micro/nano-fiber textures cured at 390 °C was willow-leaf-like (Fig. 2f), with the wider and longer size and denser nano-fiber textures than that of the lower curing temperatures (Fig. 2b and d). These obtained willow-leaf-like nano-fibers initiated great cross-linking each other and formed network with fine and long micro/nano-pores and -apertures on the micro-papillaes or -islands atop, thus the air can be trapped into the micro/nano-pores or -apertures on the coating surface minimizes the real contact area [6–10]. It led to good superhydrophobicity (the higher WCA of about 165° and the smaller WSA of about 5°) of the coating surface cured at 390 °C. When the PTFE/PPS coating cured at the highest temperature of about 400 °C, the shape of micro/nano-fiber textures changed from willow-leaf-like to wheat-haulm-leaf-like, as shown in Fig. 2(h and i). The obtained long wheat-haulm-leaf-like micro/nano-fiber textures tightly enwind around the micro-papillaes or -islands and porous network atop, which resulted in the formation of exceedingly fine and long nano-pores and -apertures. Accordingly, an increase in density of the micro/nano-fluorocarbon fiber texture peaks per unit area should answer for the increasing WCA up to about 169° (Fig. 3c) and lowering the WSA down to about 3°. The above results indicated that the curing temperature dramatically influences the shapes and sizes of the micro/nano-fiber texture of the PTFE/PPS superhydrophobic coating surfaces, leading to the increase of WCAs and the decrease of WSAs.

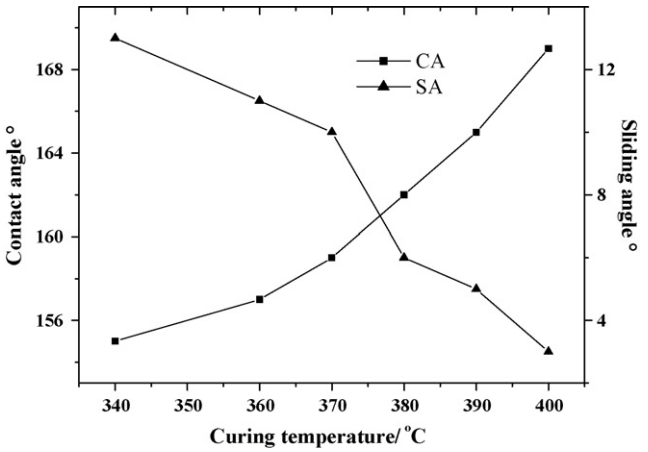

Fig. 1. Relationship between curing temperature and water contact angle or sliding angle on the PTFE/PPS superhydrophobic surfaces.

3.2. The mechanism for morphology evolution

Pristine PTFE powder cannot form stable dispersion aqueous solution and will agglomerate easily (Scheme 1a) [37]. Surface coatings prepared from the poorly dispersed PTFE solution have very large featureless micro PTFE domains and show very poor mechan-

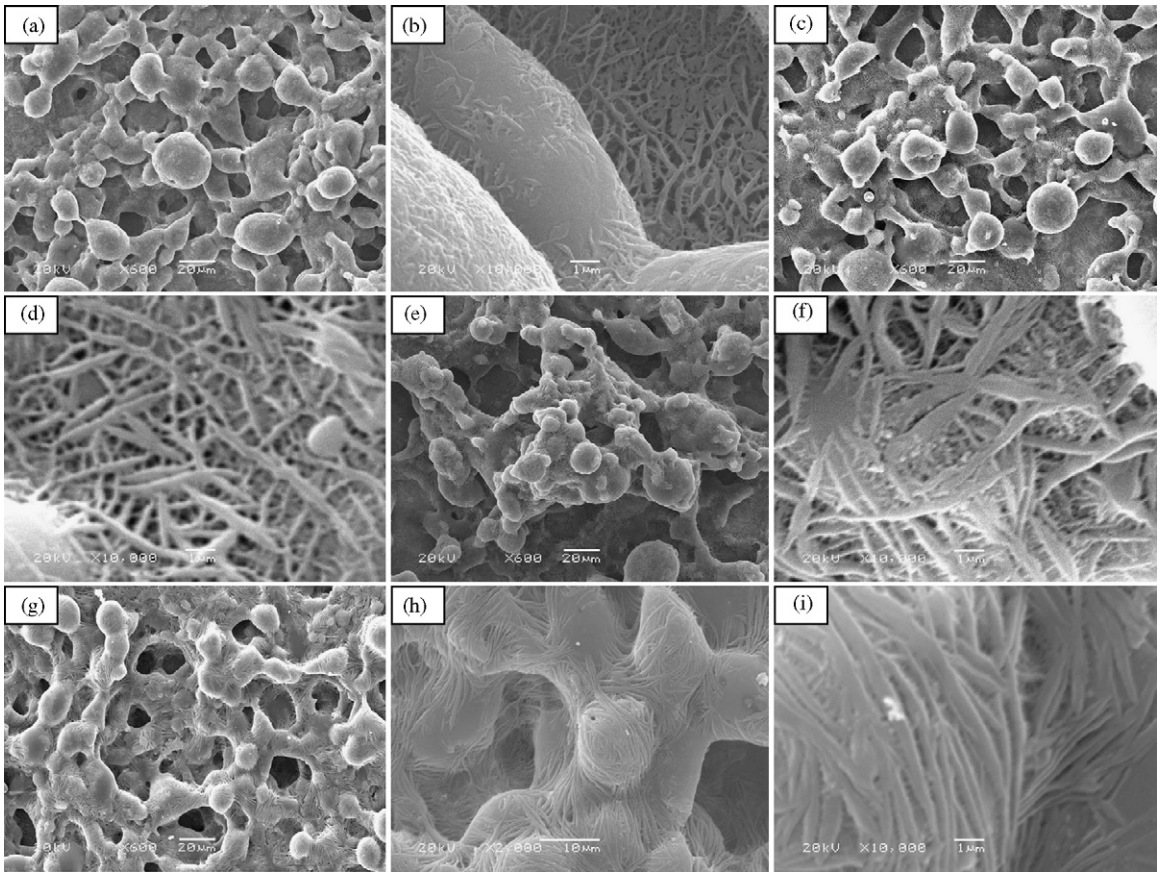

Fig. 2. SEM micrographs with different magnifications of surface microstructures of PTFE/PPS superhydrophobic coating cured at various temperature for 1.5 h, and then naturally cooled in air to room temperature: at 340 °C (a) and (b), (a. 600×, b. 10000×); at 380 °C (c) and (d), (c. 600×, d. 10000×); at 390 °C (e) and (f), (e. 600×, f. 10000×); at 400 °C (g)–(i), (g. 600×, h. 2000×, i. 10000×).

ical properties due to slippery of two phases. PTFE have very good dispersivity in the mixed solvent in the presence of non-ionic surfactant by forming PTFE emulsion (O/W), which can guarantee PTFE is uniformly blended with PPS either in solution or in pre-cured surface coatings (Scheme 1b) [38,39]. When temperature was up to about 300 °C, PTFE and PPS started to form isotropic solution. The movement of PTFE and PPS macromolecules chains was accelerated with the increasing temperature; PTFE moved gradually to the surface region, leading to fluorine (F) enrichment on top surface [40] and the enrichment of PPS at the coating/steel interface (Scheme 1c), the fact of which will be verified in following XPS measurements at both surface region and interface region. When increasing curing temperature, the PPS particles started to cross-link (Scheme 1d) [41], and surfactant around PTFE particles will be desorbed and particles merged very quickly. Higher temperature will increase the inter particle collision chance of separate particles with surrounding particles, so forming larger aggregates, while the longer cooling time and so the longer crystallization time allows growth of longer fibers. Therefore, various morphologies were obtained ranging from coils shape (~340 °C) to willow-leaf-like (~380 °C) and to wheat-haulm-leaf-like shape (~400 °C) at different curing temperatures. In a word, low curing temperature leads to short, thin fibrous morphology, and high curing temperature results in thick, long fiber growth. Moreover, the intrinsic liquid-crystal phase of PPS can also help with one dimensional fiber growth of PTFE [42–44].

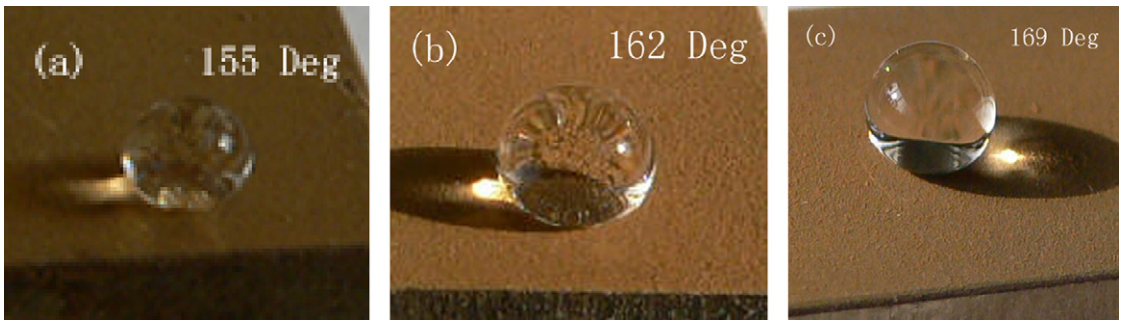

Fig. 3. Optical image of water droplets with the volume of 15 μl on the PTFE/PPS superhydophobic coating surface cured at various temperature for 1.5 h, and then naturally cooled in air to room temperature: (a) at 340 °C, (b) at 380 °C, (c) at 400 °C.

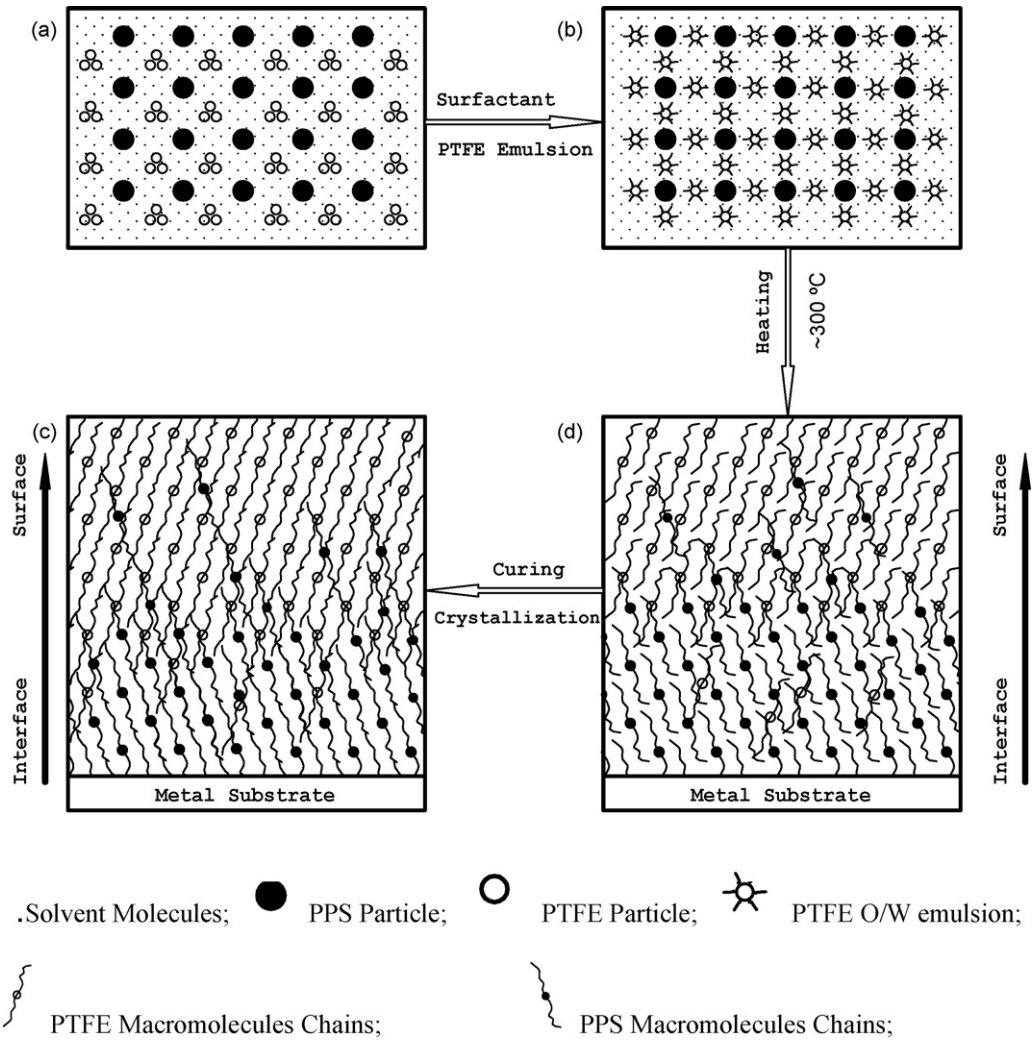

Scheme 1. The sketch map of the mechanism of the dispersion and macromolecular-dynamics. The dispersion of the original PTFE powder (a) and PTFE O/W emulsion (b); the macromolecules chains thermo-movement (c) and entanglement or cross-linking (d).

3.3. The control of the gradient-distribution by curing temperature

XPS analyses of C1s, F1s, Ols, and S2p were performed on PTFE/PPS superhydrophobic coating (40 vol.% PTFE) surface and interface at stainless steel cured at various temperatures, respectively. As shown in Fig. 4, the XPS of the coating surface (Fig. 4a) exhibits strong Cls peak at 293.8 eV binding energy [45] (C_I, C-F_3) and a small peak at around 285 eV (C_{II}, Ph-S). The intensity of the Cls peaks on the interface (Fig. 4b) was contrary to that of the surface (Fig. 4a), i.e., the intensity of the Cls peak at 293.7 eV (C_I, C-F_3) and at 285 eV (C_{II}, Ph-S) gradually decreased and increased from coating surface to interface cured at various temperatures, respectively (Fig. 4c and d). As shown in Table 1, the atom content of F of the surface cured at various temperatures is higher than that of in the interface, but the atom content of O and S of surface cured at various temperatures are lower than that of in the interface; that is, the F(ls)/S(2p) and C_I/C_{II} ratio decreased sharply from coating surface to interface, respectively. For the curing process, PTFE started to form isotropic solution and shifted gradually from coating interior to surface leading to fluorine (F) enrichment on the top surface. So, the gradient-distribution of fluorine resulted in the main possession of PTFE in the coating surface and PPS in the interface. It greatly confirmed the mechanism of the macromolecular-dynamics (Scheme 1c). Furthermore, with the temperature increased up to about 340 °C, PPS isotropic solution started to generate thermal-oxidative cross-linking and oxidative reaction, resulting in –C=O, –C–O and –S=O, O=S=O functional groups respectively (shown in Fig. 4b and d, and Table 1) [46]. It led to enhanced adhesion between stainless steel substrate and PTFE/PPS coatings which was explained by the formation of electron acceptor groups (–C=O, C–O and –S=O, O=S=O) in PPS polymer and electron donors in metal [47,48]. Moreover, it is helpful in enhancing adhesive strength between PTFE macromolecule chain and PPS macromolecule chain, resulting in outstanding mechanical properties of the coatings.

With the curing temperature increased from 340 °C to 400 °C, the intensity of the Fls peak of surface gradually increased (Fig. 4c); while the atom content of F in interface (Fig. 4d) gradually decreased (Table 1, from 50.4 at.% to 27.3 at.%), and the atom content of O of interface sharply increased (Fig. 4d and Table 1, from 2.9 at.% to 33.8 at.%). As we know, with the curing temperature increasing, PTFE isotropic solution greatly entangled [41] and shifted largely from coating interior to surface leading to richer fluorine (F) on the atop surface, resulting in the enhancement of the fluorine gradient-distribution (Fig. 4c and d). The stronger thermal-oxidative cross-linking and oxidative reaction of PPS macromolecule chain led to the increase of –C=O, –C–O and –S=O, O=S=O functional groups on the interface (Fig. 4b and d,

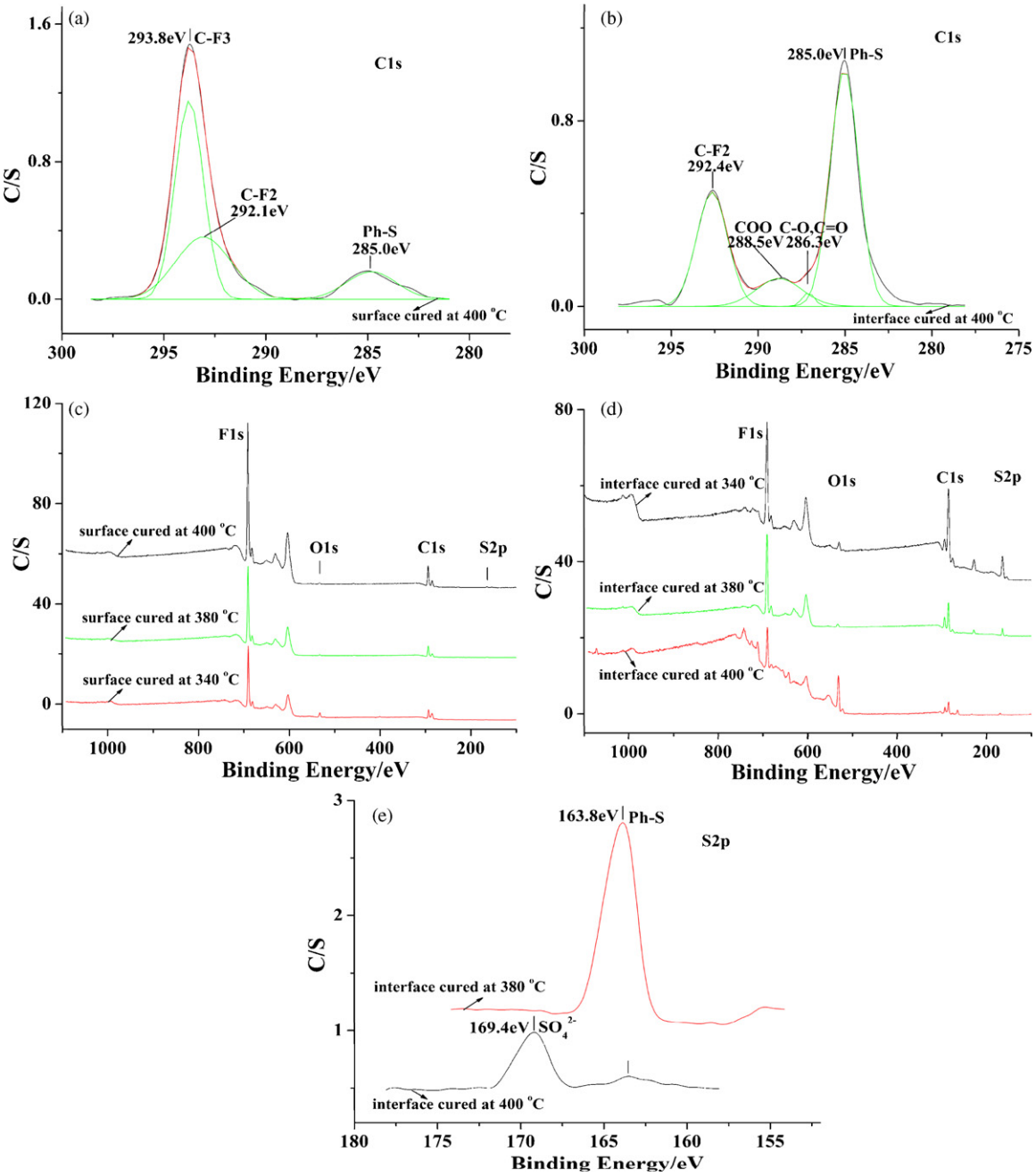

Fig. 4. XPS spectra of the 40 vol.% PTFE/PPS superhydrophobic coating cured at various temperature: (a) XPS C1s core-level spectra of the superhydrophobic coating surface, (b) interface between coating and stainless steel substrate, (c) XPS survey spectra of the coating surface and (d) interface, (e) XPS S2p spectra of the coating interface between coating and stainless steel substrate.

and Table 1), thus greatly enhanced adhesion between stainless steel substrate and PTFE/PPS coatings. Therefore, increasing the curing temperature can benefit in fluorine gradient-distribution, PPS thermal-oxidative cross-linking and oxidative reaction, which results in the enhancement of adhesive strength and mechanical properties of the PTFE/PPS superhydrophobic coatings.

When the PTFE/PPS superhydrophobic coatings cured at the highest temperature up to 400 °C (decomposing temperature

Table 1
XPS analyses data of 40 vol.% PTFE/PPS superhydrophobic coating surface and interface under various curing temperatures.

Sample of curing at various temperatures	F (at.%)	C_I (%) (292–294 eV)	C_{II} (%) (285 eV)	O (%)	S (%)
Surface cured at 340 °C	71.9	18.7	8.5	0.2	0.6
Interface cured at 340 °C	52.8	15.2	22.4	3.4	6.2
Surface cured at 380 °C	73.0	20.4	5.6	0.8	0.2
Interface cured at 380 °C	50.4	13.9	29.4	2.9	3.4
Surface cured at 400 °C	74.2	22.2	2.5	1.0	0.1
Interface cured at 400 °C	27.3	7.4	14.7	33.8	1.2

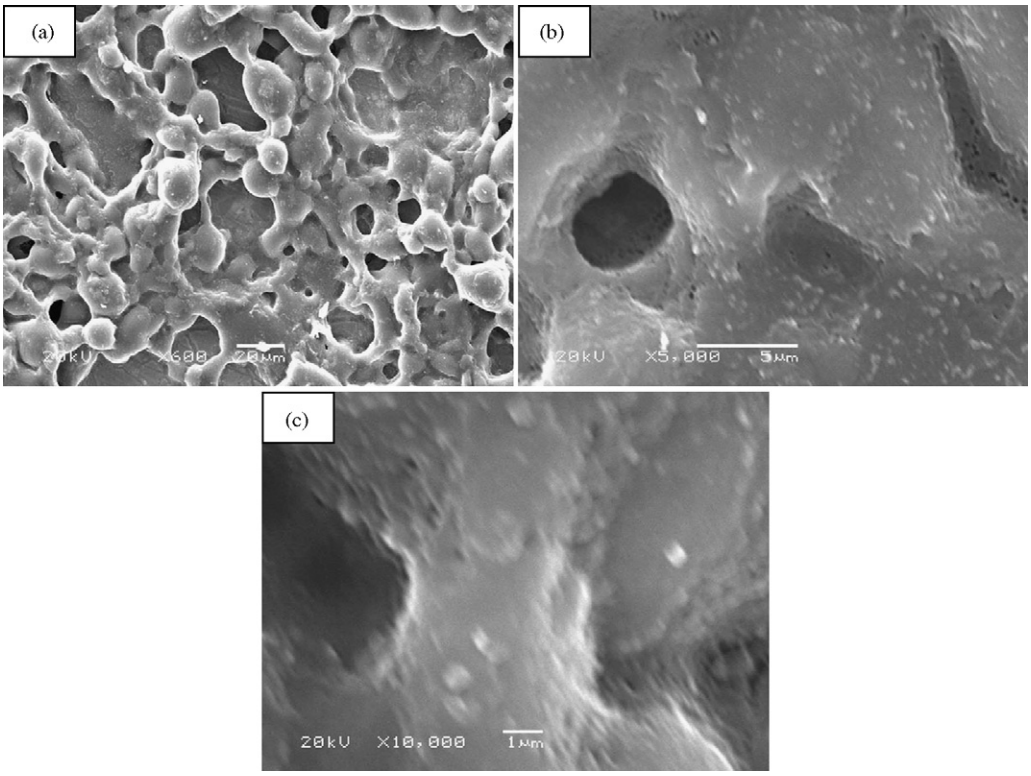

Fig. 5. SEM micrographs with different magnifications of surface microstructures of PTFE/PPS superhydrophobic coating cured at 380 °C and then hardening in H_2O, (a. 600×, b. 5000×, c. 10000×).

of PPS), PPS isotropic solution on the interface decomposed and reacted thermo-chemically (Fig. 4e) regardless of thermal-oxidative cross-linking. As shown in Fig. 4e, the S2p peak at 163.8 eV, referring to Ph-S, is observed for the coating interface both cured at 380 °C and at 400 °C, respectively. While a new S2p peak at 169.4 eV on the coating interface cured at 400 °C (Fig. 4e) indicates that S is possibly linked with O to generate SO_4^{2-}, which resulted from the thermal oxidation effect [49]. Thus it is concluded that the higher curing temperature (about 400 °C) could lead to decomposition and oxidation of S on the PTFE/PPS coating interface; the generated active S reacts thermo-chemically with substrate Fe, atmospheric O and H_2O, with the generation of $FeSO_4$ or $Fe_2(SO_4)_3$ [49]. The resulted $FeSO_4$ or $Fe_2(SO_4)_3$ on the interface leads to further enhanced adhesive strength between stainless steel substrate and coatings [49].

3.4. The control of the MNBS and gradient-distribution by cooling process

In order to demonstrate the mechanism of the creation of micro-nano-scale binary structures, the effect of the cooling process on the MNBS roughness was investigated. The PTFE/PPS superhydrophobic coatings were prepared by curing at 380 °C for 1.5 h and then put into H_2O for hardening. Fig. 5 shows the SEM micrographs of surface microstructures of PTFE/PPS superhydrophobic coating cured at 380 °C and then hardening in H_2O. The results clearly show that the porous network and micro-papillaes or -islands microstructures (Fig. 5a) of the surface were very similar to that of cured at 380 °C for 1.5 h and then naturally cooled in air to room temperature (Fig. 2c), indicating that the formation of the porous network micro-structure of the PTFE/PPS superhydrophobic coating surface was irrelative to the curing temperature and cooling process. However, it might be attributed to the mixed solvent evaporating (~150 °C) [15], the decomposing and volatilizing of $(NH_4)_2CO_3$ [15] and the surfactant expanding [50,51] slowly under heating process (150–300 °C).

As shown in Fig. 5(b and c), the porous network and micro-papillaes or -islands surfaces were covered with the micro/nano-fluorocarbon papillaes textures of 200–800 nm in diameter instead of the micro/nano-fiber textures as shown in Fig. 2(d, f, h and i), resulting in lower WCAs (about 152°) and larger WSAs (no sliding angle) than that of produced by natural cooling in air (Fig. 1). That is becauase being hardened in H_2O, the temperature sharply lowered from 380 °C to room temperature during a few seconds, the formation of PTFE aggregates could not promptly produce the crystallization and create the micro/nano-fiber on the atop surface. In fact, the micro/nano-fiber textures of the superhydrophobic surfaces should be fabricated by crystallizing of PTFE aggregates during longer cooling process. That is, the formation of the micro/nano-fibers could take place by means of a liquid-crystal 'templating' mechanism [42–44]. Accordingly, a bionic superhydrophobic surface with porous gel-like network and micro/nano-fiber textures could be created by natural cooling instead of prepared by hardening in H_2O.

XPS analyses of C1s, F1s, Ols, and S2p were performed on PTFE/PPS superhydrophobic coatings (40 vol.% PTFE) surface and interface cured at 380 °C and then hardening in H_2O (Fig. 6). From Fig. 6, it is clear that the trends of the element composition and content as well as the gradient-distribution of the surface or interface by hardening in H_2O were very similar with that of produced by natural cooling in air as shown in Fig. 6(a–d). However, the atom content of F (37.1 at.%) and C (C-F_2, 9.3 at.%) in interface by hardening in H_2O was lower than that of produced by natural cooling in air (50.4 at.% and 13.9 at.%, respectively), as listed in Table 2; while the atom content of O (12.2 at.%) of interface by hardening in H_2O was higher than that of natural cooling in air (2.9 at.%) as

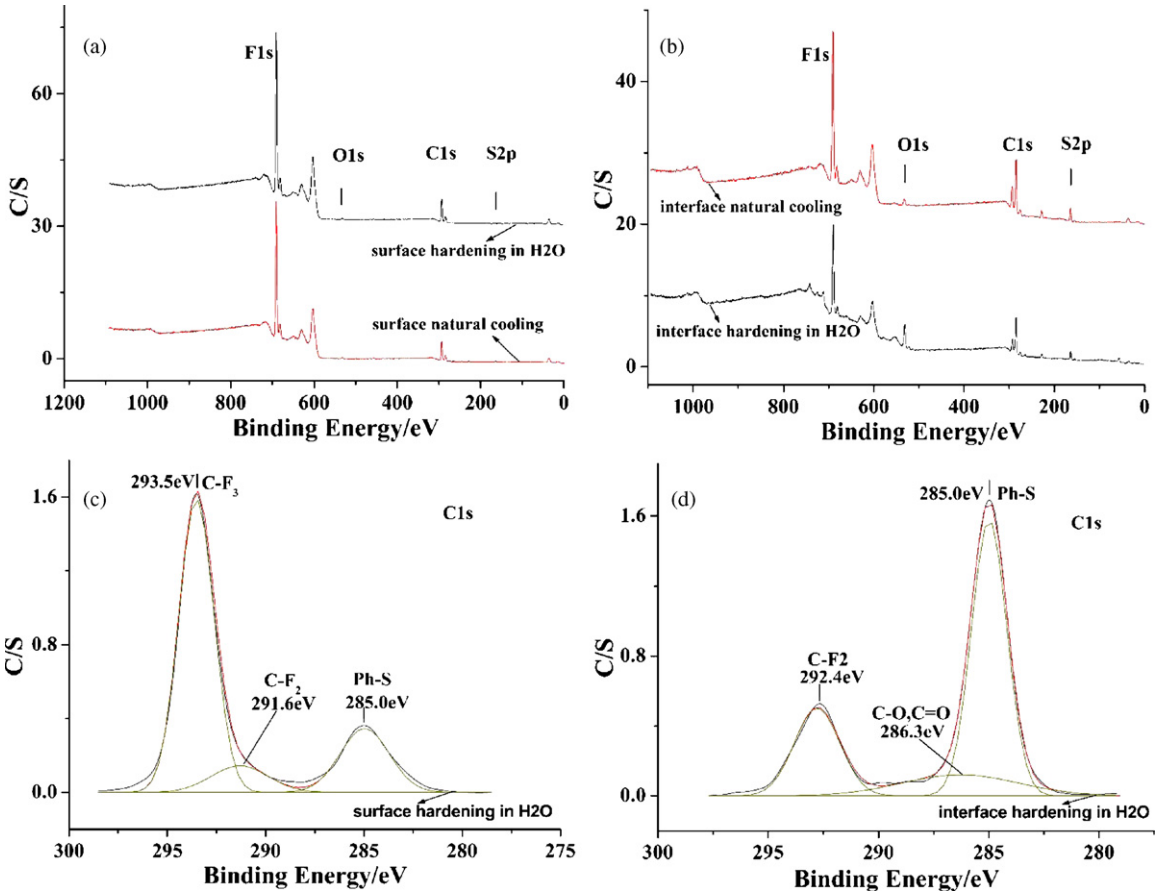

Fig. 6. XPS spectra of the 40 vol.% PTFE/PPS superhydrophobic coating cured at 380 °C for 1.5 h and then hardening in H_2O: (a) XPS survey spectra of the coating surface and (b) interface, (c) XPS C1s core-level spectra of the coating surface, (d) interface between coating and stainless steel substrate.

Table 2
XPS analyses data of 40 vol.% PTFE/PPS superhydrophobic coating surface and interface cured at 380 °C for 1.5 h, and cooled at various conditions.

Sample: coating of various curing-conditions	F (at.%)	C_I (%) (292–294 eV)	C_{II} (%) (285 eV)	O (%)	S (%)
Surface of naturally cooling	73.0	20.4	5.6	0.8	0.2
Interface of naturally cooling	50.4	13.9	29.4	2.9	3.4
Surface of hardening in H_2O	73.3	20.1	5.3	1.1	0.2
Interface of hardening in H_2O	37.1	9.3	29.9	12.2	2.9

shown in Fig. 6(b and d) and Table 2. All these results illustrated that the enhancement of the cohesion-strength on the interface was obtained by means of hardening in H_2O [46–48].

4. Conclusions

In conclusion, a simple and conventional coating-curing process to fabricate superhydrophobic coating surface with both the MNBS roughness, and the lowest surface energy hydrophobic groups (-CF_3) on engineering materials of stainless steel or other metals was developed by control of curing conditions.

A higher curing temperature and longer cooling time resulted in longer crystallizing process, which is beneficial to create the willow-leaf-like or wheat-haulm-leaf-like micro/nano-fiber on the atop surface with superhydrophobic ability. The curing temperature dramatically influences the micro/nano-fiber texture of the PTFE/PPS superhydrophobic coating surface; higher curing temperature leads to the increase of WCAs and the decrease of WSAs. An increase of curing temperature is helpful to fluorine gradient-distribution, PPS thermal-oxidative cross-linking and oxidative reaction, resulting in the enhancement of adhesive strength and mechanical properties of the PTFE/PPS superhydrophobic coatings.

The mico/nano-fiber textures of the superhydrophobic surface could be fabricated by crystallizing of PTFE aggregates during a longer cooling process. A bionic superhydrophobic surface with porous gel-like network and micro/nano-fiber textures could be created by natural cooling in air but could not be prepared by hardening in H_2O.

Acknowledgments

The authors thank the National 973 project (No.2007 CB607601), the National Natural Science Foundation of China (No. 50835009) and the Innovative Group Foundation of NSFC (Grant No. 50721062) for financial support, and Prof. Feng Zhou for instructive and fruitful discussions.

References

[1] L. Feng, Y. Song, J. Zhai, B. Liu, J. Xu, L. Jiang, D. Zhu, Angew. Chem. Int. Ed. 42 (2003) 800.
[2] H.S. Lim, D.H. Kwak, D.Y. Lee, S.G. Lee, K. Cho, J. Am. Chem. Soc. 129 (2007) 4128.
[3] X.J. Feng, L. Jiang, Adv. Mater. 18 (2006) 3063.
[4] J.Y. Shiu, C.W. Kuo, P. Chen, C.Y. Mou, Chem. Mater. 16 (2004) 561.
[5] X.M. Li, D. Reinhoudt, M. Crego-Calama, Chem. Soc. Rev. 36 (2007) 1350.

[6] W. Barthlott, C. Neinhuis, Planta 202 (1997) 1.
[7] Z.G. Guo, F. Zhou, W.M. Liu, J.C. Hao, J. Am. Chem. Soc. 127 (2005) 15670.
[8] Z.G. Guo, W.M. Liu, Plant Sci. 172 (2007) 1103.
[9] W. Liab, A. Amirfazli, Soft Matter 4 (2008) 462.
[10] X. Zhang, F. Shi, J. Niu, Y.G. Jiang, Z.Q. Wang, J. Mater. Chem. 18 (2008) 621.
[11] M. Li, H. Schnablegger, S. Mann, Nature 402 (1999) 393.
[12] J.D. Hartgerink, E. Beniash, S.I. Stupp, Science 294 (2001) 1684.
[13] J.F. Zheng, A.H. He, J.X. Li, J. Xu, C.C. Han, Polymer 47 (2006) 7095.
[14] Z.G. Guo, W.M. Liu, Appl. Phys. Lett. 90 (2007) 223111.
[15] J.T. Han, S.Y. Kim, J.S. Woo, G.W. Lee, Adv. Mater. 20 (2008) 3724.
[16] T.L. Sun, H. Tan, D. Han, Q. Fu, L. Jiang, Small 1 (2005) 959.
[17] G.M. Chapman, H. Bai, C. Li, G.Q. Shi, Mater. Chem. Phys. 114 (2009) 120.
[18] A. Synytska, D. Appelhans, Z.G. Wang, F. Simon, F. Lehmann, M. Stamm, K. Grundke, Macromolecules 40 (2007) 297.
[19] L. Zhai, F.C. Cebeci, R.E. Cohen, M.F. Rubner, Nano. Lett. 4 (2004) 1349.
[20] J.J. Lin, C.C. Chu, C.C. Chou, F.S. Shieu, Adv. Mater. 17 (2005) 301.
[21] N.J. Shirtcliffe, G. McHale, M.I. Newton, C.C. Perry, P. Roach, Mater. Chem. Phys. 103 (2007) 112.
[22] T. Minami, H. Mayama, S. Nakamura, S. Yokojima, J.W. Shen, K. Tsujii, Soft Matter 4 (2008) 140.
[23] S. Chen, C.H. Hu, L. Chen, N.P. Xu, Chem. Commun. 19 (2007) 19.
[24] D. Nystrom, J. Lindqvist, E. Östmark, A. Hult, E. Malmström, Chem. Commun. (2006) 3594.
[25] L. Ghannam, M. Manguian, J. Francois, L. Billon, Soft Matter 3 (2007) 1492.
[26] Y. Coffinier, S. Janel, A. Addad, R. Blossey, L. Gengembre, E. Payen, R. Boukherroub, Langmuir 23 (2007) 1608.
[27] Y. Zhao, Q. Lu, D.S. Chen, Y. Wei, J. Mater. Chem. 16 (2006) 4504.
[28] M.L. Ma, M. Gupta, Z. Li, L. Zhai, K.K. Gleason, R.E. Cohen, M.F. Rubner, G.C. Rutledge, Adv. Mater. 19 (2007) 255.
[29] H.Y. Erbil, A.L. Demirel, Y. Avci, O. Mert, Science 299 (2003) 1377.
[30] B. Liu, Y.N. He, Y. Fan, X.G. Wang, Macromol. Rapid Commun. 27 (2006) 1859.
[31] Y. Zhu, J.M. Li, M.X. Wan, L. Jiang, Polymer 49 (2008) 3419.
[32] Y. Ma, X.Y. Cao, X.J. Feng, Y.M. Ma, H. Zou, Polymer 48 (2007) 7455.
[33] J.J. Lin, C.C. Chu, M.L. Chiang, W.C. Tsai, Adv. Mater. 18 (2006) 3248.
[34] H.J. Song, Z.Z. Zhang, X.H. Men, Appl. Phys. A 91 (2008) 73.
[35] Z.Z. Luo, Z.Z. Zhang, L.T. Hu, W.M. Liu, Z.G. Guo, H.J. Zhang, W.J. Wang, Adv. Mater. 20 (2008) 970.
[36] Z.Z. Luo, Z.Z. Zhang, W.J. Wang, W.M. Liu, Surf. Coat. Technol. 203 (2009) 1516.
[37] J. Tian, Y.L. Huang, J. Appl. Polym. Sci. 86 (2002) 3454.
[38] L. Vaisman, H.D. Wagner, G. Marom, Adv. Colloid. Interfac. Sci. 128–130 (2006) 37.
[39] J. Zou, B.H. Ji, X.Q. Feng, H.J. Gao, Small 2 (2006) 1348.
[40] D.J. Walbridge, Prog. Org. Coat. 28 (1996) 155.
[41] M. Rubinstein, R.H. Colby, Polymer Physics, Oxford, New York, 2004.
[42] C.T. Kresge, M.E. Leonowicz, W.J. Roth, Nature 359 (1992) 710.
[43] J. Yu, Y.J. Qiu, X.X. Zha, M. Yu, J.L. Yu, J. Rafique, J. Yin, Eur. Polym. J. 44 (2008) 2838.
[44] M.G. Buonomenna, A. Gordano, E. Drioli, Eur. Polym. J 44 (2008) 2051.
[45] S.R. Coulson, I. Woodward, J.P.S. Badyal, J. Phys. Chem. B 104 (2000) 8836.
[46] T.R. Hawkins, Macromolecules 9 (1976) 189.
[47] S.K. Koh, W.K. Choi, J.S. Cho, S.K. Song, J. Mater. Res. 11 (1996) 2933.
[48] J.S. Cho, Y.W. Beag, S. Han, K.H. Kim, C. Cho, S.K. Koh, Surf. Coat. Technol. 128–129 (2000) 66.
[49] L.G. Yu, S.R. Yang, Thin Solid Films 413 (2002) 98.
[50] V.B. Fainerman, D. Mobius, R. Miller, Surfactants: Chemistry, Interfacial Properties, Applications, Elsevier, Netherlands, 2001.
[51] J.H. Clint, Surfactant Aggregation, Blackie, London, 1992.